scientific reports

Check for updates

OPEN

Shear strength characteristics of basalt fiber-reinforced loess

Chong-kun Chen[1], Gang Li[1]✉, Jia Liu[2], Yu Xi[1] & Jing-jing Nan[1]

Loess owns the characteristics of collapsibility, disintegration and solubility, which pose a challenge to engineering construction. To examine the shear strength of basalt fiber-reinforced (BFR) loess, consolidated undrained (CU) triaxial tests were conducted to explore the impacts of water content (*w*), fiber length (*FL*), fiber content (*FC*) and cell pressure (σ_3) on the shear strength. According to the results, the shear strength model was established taken into account the impacts of *FL*, *FC*, and fiber diameter (*d*). The results showed that the peak strength of BFR soils enhanced as *FL*, *FC*, and σ_3 increasing, whereas it decreased with increasing of *w*. Compared to unreinforced soil, the peak strength of BFR loess improved 64.60% when *FC* was 0.2% and *FL* was 16 mm. The optimum reinforcement condition for experimental loess was that of *FL* was 16 mm and *FC* was 0.8%. The reinforcing mechanism of fibers was divided into a single tensile effect and spatial mesh effect. The experimental and calculated results agreed well, which suggested the model is suitable for predicting the shear strength of BFR loess. The research results can offer a guideline for the application of BFR loess in the subgrade and slope engineering.

Loess is Quaternary sediment that is widespread in the northwest of China[1]. With the development of the "Belt and Road Initiative," modern transportation facilities represented by highways and high-speed railways have been built in large numbers[2–4]. However, the structural features of loess, such as porous, weakly cemented, and under compacted, lead to collapsibility, disintegration, and solubility, which pose a challenge to engineering construction[5]. Fiber reinforcement (FR) method provides an idea to solve engineering problems, and the fibers limit deformation of soil particles through the tensile force and frictional force, resulting in excellent mechanical properties of reinforced soil[6,7]. Ibraim et al.[8–10] concluded that the compaction energy of loose fiber-reinforced sand is less than denser unreinforced sand when the peak strength keeps constant. The fiber-reinforced method can significantly reduced the liquefaction potential of sand in compression and extension loadings. A new sampling method for fiber-reinforced sand adopted vibration of moist sand/fiber mixtures was proposed and assessed. Reza Tabakouei et al.[11] stated that the fiber type, fiber length, and specimen diameter determined the unconfined compression strength of fiber-reinforced sandy soil. Sharma and Kumar[12] reported that the relative density remarkably affects the ultimate bearing capacity and settlement of fiber-reinforced sand, and the improvement effect reached maximum when relative density was 70%. Festugato et al.[13] reported that inclusion of polypropylene fiber changed the dense sand stiffer than the unreinforced sand under cyclic loading. Choobbasti et al.[14] concluded that polyvinyl alcohol fiber can improved the shear strength and axial strain at failure of Babolsar sand, while decreased the strength loess after peak strength. Soriano et al.[15] discovered that the porosity of fiber-reinforced sand increased in the fiber vicinity, which validated the assumption of stolen void ratio. Mandolini et al.[16] stated that the fiber strength governed by tensile strain domain and fiber orientation distribution.

For clayey soil, Abdi et al.[17] concluded that polypropylene fiber can increased the compression, strength, and ductility of clay-lime composites. Hejazi et al.[18] reported that the fiber content, fiber diameter, and fiber aspect ratio affected the shear strength of fiber-reinforced soil. Abbaspour et al.[19] revealed that the waste tire textile fibers can improved the mechanical properties of expansive soil, and the swelling deformations was reduced by 44%. Consoli et al.[20,21] reported that the ratio of porosity and cement played a critical role in evaluate the unconfined compression strength of fiber-reinforced soil–lime composites. Furthermore, the addition of fiberglass was ineffective to deduce the volumetric strain of fiber-reinforced sulfate-rich dispersive soil. Tamassoki et al.[22] stated that 3% content of activated carbon and coir fiber can significantly improved the compressive strength, while 2% content can remarkably enhanced the shear strength of lateritic soil. Soleimani-Fard et al.[23] revealed that discrete distributed fibers can significantly improved the shear strength, compressive, and hydraulic conductivity of fiber-reinforced fine-grained soil. Malekzadeh and Bilsel[24] reported that the addition of polypropylene fiber can significantly decreased the swell-shrink of expansive soil, and shrinkage limit increased more than 50%.

[1]Shaanxi Key Laboratory of Safety and Durability of Concrete Structures, Xijing University, Xi'an 710123, Shaanxi, China. [2]School of Geological Engineering and Geomatics, Chang'an University, Xi'an 710054, Shaanxi, China. ✉email: T_bag945@126.com

Phanikumar and Singla[25] stated that the swell potential and swelling pressure of nylon fiber-reinforced expansive soil decreased with fiber length increased, and the secondary consolidation properties significantly enhanced for fiber-reinforced soil. Wang et al.[26] concluded that the compressive and tensile strengths of collapsibility loess showed the trends of first increased then decreasing as increasing of glass fiber content (*FC*). Huang et al.[27] found the FR can remarkably enhance the strength of remodeled loess. At the same time, the compressive modulus first increased then decreased with increasing *FC*, and the optimal *FC* was 0.6%. Xu et al.[28] declared that the damage deviator stress of basalt FR (BFR) loess enhanced firstly and then reduced as *FC* increased, and the optimal *FC* was 0.6%. Zhu et al.[29] found that the optimum condition for the unconfined compressive strength (UCS) of polypropylene FR loess with fiber length (*FL*) and *FC* was 12 mm and 0.5%, respectively. Meanwhile, the optimum condition for the deformation modulus was 12 mm *FL* and 0.3% *FC*. Zuo et al.[30] adopted composite method to modify the soil, and they concluded that the compressive strength and flexibility of loess were effectively improved, and the optimal conditions were 1.5% of xanthan gum and 0.6% of basalt fiber. Lu et al.[31] declared that the shear strength indices of polypropylene FR loess enlarged by 113.8% and 23.3%, respectively, whereas the disintegration rate decreased nearly 87.5%. An et al.[32] observed the permeable ability of polypropylene FR soil increased significantly, and the protective effect of the loess slope was evident. Dong et al.[33] found that the strength of lignin FR soil enhanced as cell pressure (σ_3) increased, and the stress–strain curve transferred from hardening to softening with increasing *FC*. Chu et al.[34] obtained that the strength of FR soil rose firstly, then reduced as increasing of *FC*, and the cohesion increased remarkably. Xiong et al.[35] observed that the curves of BFR loess were converted from softening to hardening, and the shear strength indices were improved by 52.03% and 24.30%, respectively. Wang et al.[36] concluded that basalt fibers can significantly improve the loess creep, and the creep deformation of BFR soils decreased with increasing σ_3. Hu et al.[37] noted the cohesion of FR loess enhanced firstly and subsequently reduced with increasing *FC*, and the optimal *FC* should be at least 0.2% in practical engineering. Gao et al.[38] found that the UCS of samples prepared by the dilute mixing method was more suitable than that of the direct mixing method, and the effect of lignin *FC* on UCS was more obvious. Su and Lei[39] pointed out that palm fiber can remarkably improve UCS of loess, and the influence of dry density on strength is significant, while the impact of *FL* is not significant. Chen et al.[40] declared that the dynamic shear modulus of loess enlarged remarkably with raising fly ash content and cell pressure, whereas the damping ratio decreased as increasing fly ash content and σ_3. Yang et al.[41] found that the polypropylene fibers can change the cement-modified loess from brittle to plastic damage, and the fibers played a bridging role. The optimal reinforcement conditions were 0.30–0.45% of *FC* and 12 mm of *FL*.

Basalt fiber is a green inorganic composite material with high strength, temperature resistance, corrosion resistance, and no pollution, which has good application prospects in the fields of aerospace, manufacturing, and civil engineering. In order to validate the effective of basalt fiber-reinforced method, and establish a shear strength model of BFR loess. Based on consolidated undrained (CU) test, the effects of water content (w), *FL*, *FC*, and σ_3 were analyzed, and the reinforced mechanism was revealed by loess microstructure used scanning electron microscopy (SEM). Furthermore, a shear strength model of BFR loess considering the effects of *FL*, *FC*, and fiber diameter (d) was established. The results can offer great guideline to applications of BFR soils.

Materials and methods

Experimental materials

The Loess was obtained from Yan'an (Shaanxi, China) in a construction site with a depth of 2.5 m, and Table 1 lists the basic parameters of loess. It can be found that experimental loess has the characteristics of low water content and large void ratio, which can be classified as silty clay. For engineering construction, loess foundation generally needs to solidify to improved the bearing capacity and reduce the settlement.

Basalt fiber was bought from Shijiazhuang Zhuzhong Technology Co., Ltd (Hebei, China). The diameter and density of basalt fiber was 10 μm and 2.65 g/cm^3, the tensile strength nearly 4000 MPa, and the elastic modulus reached 100 GPa.

Sample preparation

During the sample preparation progress, the remolded loess was firstly smashed, and then sieved with a 2-mm griddle. The sample density was set as 1.45 g/cm^3. The basalt fiber is disassembled into filiform, and the fixed length and content of fibers are evenly mixed with dry soil by electric blender to ensure the uniform distribution

Physical characteristics	Values
Specific gravity, G_s	2.67
Dry density, ρ_d (g/cm^3)	1.13
Water content, w (%)	9.00
Void ratio	0.83
Liquid limit, w_L (%)	25.00
Plastic limit, w_P (%)	12.00
Plasticity index, I_p	13.00

Table 1. Physical characteristics of loess.

of fibers. Subsequently, a certain amount of water was adding to the blend fiber-reinforced soil and put in a glass container for 24 h. The sample size was 50 mm (diameter) × 100 mm (height), and it was produced by five levels.

Experimental methodology

To investigate shear strength characteristics of BFR soil, the CU experiments were carried out by triaxial instrument. According to the standard for soil test method (GB/T 50,123–2019)[42], tests were conducted at 0.5%/min strain rate, and were ceased at 20% axial strain. Table 2 lists the test program, 102 group experiments were carried out. The degree of saturation corresponded to 9% *w* and 13% *w* were 28.95% and 41.82%, respectively.

Results and discussion

Stress–strain curves of BFR loess

Analysis of the Effect of w

The water content had greater impact on mechanical characteristics of loess, while it impact on the FR soils deserves further study. Figure 1 shows the stress–strain curves of BFR soil with *FL* of 4 mm, 8 mm, 12 mm, and 16 mm under 25 kPa σ_3. The peak deviator stress decreased with increasing *w*, and the peak strength of BFR loess is higher than that of loess, which consistent with reference[43]. For the unreinforced loess, the peak strength decreased by 31.65% at 13% *w* compared to 9% *w* under 4 mm *FL*. While for the BFR soils, the peak strength decreased by 20.38% and 12.93% at 13% *w* compared to 9% *w* when *FC* was 0.2% and 0.6%, respectively. The difference of deviatoric stress between 9 and 13% *w* at 0.2% *FC* was significantly larger than that of at 0.6% *FC*. The main reason is that fiber can improved the strength by limit the deformation of soil particles through the tensile force and frictional force, and the reinforcement effect at high *FC* was significantly larger than that of at low *FC*. Therefore, the difference of deviatoric stress between 9 and 13% *w* decreased with increasing *FC*.

Analysis of the effect of FL

The Fig. 2 shows the stress–strain curves of BFR soil with *w* of 9% and *FC* of 0.2%, 0.4%, 0.6%, and 0.8% under 25 kPa σ_3. The curves of loess showed a strain-softening, whereas the BFR loess exhibited a strain-hardening[44]. The peak deviator stress of BFR soil increased as increasing of *FL*. Compared to unreinforced soil, the peak strength with *FC* of 0.2% and *FL* of 4 mm, 8 mm, 12 mm, and 16 mm increased by 17.21%, 28.97%, 40.45%, and 64.60%, respectively. The main reason is that fibers are randomly and uniformly distributed between the soil particles to form a composite that bears the loading together, resulting in significantly improved shear strength of BFR loess. As *FL* increased, the touch-points between fibers and soil particles increased results in the improvement of anchor effect. The restrain effect between the soil particles enhanced due to the stretching and flexible constraining by the fibers[45].

Analysis of the Effect of FC

The Fig. 3 shows the stress–strain curves of BFR loess with *w* of 9% and *FL* of 4 mm, 8 mm, 12 mm, and 16 mm under 25 kPa σ_3. The peak strength of BFR loess enhanced gradually by increasing *FC*, which is consistent with the results of references[46]. Compared to loess, the BFR soil with *FL* of 4 mm and *FC* of 0.2%, 0.4%, 0.6%, and 0.8%, the peak strength raised by 17.21%, 27.55%, 42.73%, and 60.66%, respectively. The main reason to explain the phenomenon is that with increasing of *FC*, the fiber number increased, which resulted in the more contact points between fiber and soil particles. Due to fibers can limit deformation of soil particles through anchoring effect, thereby result in improved the sample strength and prevent sample damage[22,23].

σ_3 (kPa)	*w* (%)	*FL* (mm)	*FC* (%)
25	9, 13	0	0
25	9, 13	4	0.2, 0.4, 0.6, 0.8
25	9, 13	8	0.2, 0.4, 0.6, 0.8
25	9, 13	12	0.2, 0.4, 0.6, 0.8
25	9, 13	16	0.2, 0.4, 0.6, 0.8
50	9, 13	0	0
50	9, 13	4	0.2, 0.4, 0.6, 0.8
50	9, 13	8	0.2, 0.4, 0.6, 0.8
50	9, 13	12	0.2, 0.4, 0.6, 0.8
50	9, 13	16	0.2, 0.4, 0.6, 0.8
100	9, 13	0	0
100	9, 13	4	0.2, 0.4, 0.6, 0.8
100	9, 13	8	0.2, 0.4, 0.6, 0.8
100	9, 13	12	0.2, 0.4, 0.6, 0.8
100	9, 13	16	0.2, 0.4, 0.6, 0.8

Table 2. Test program.

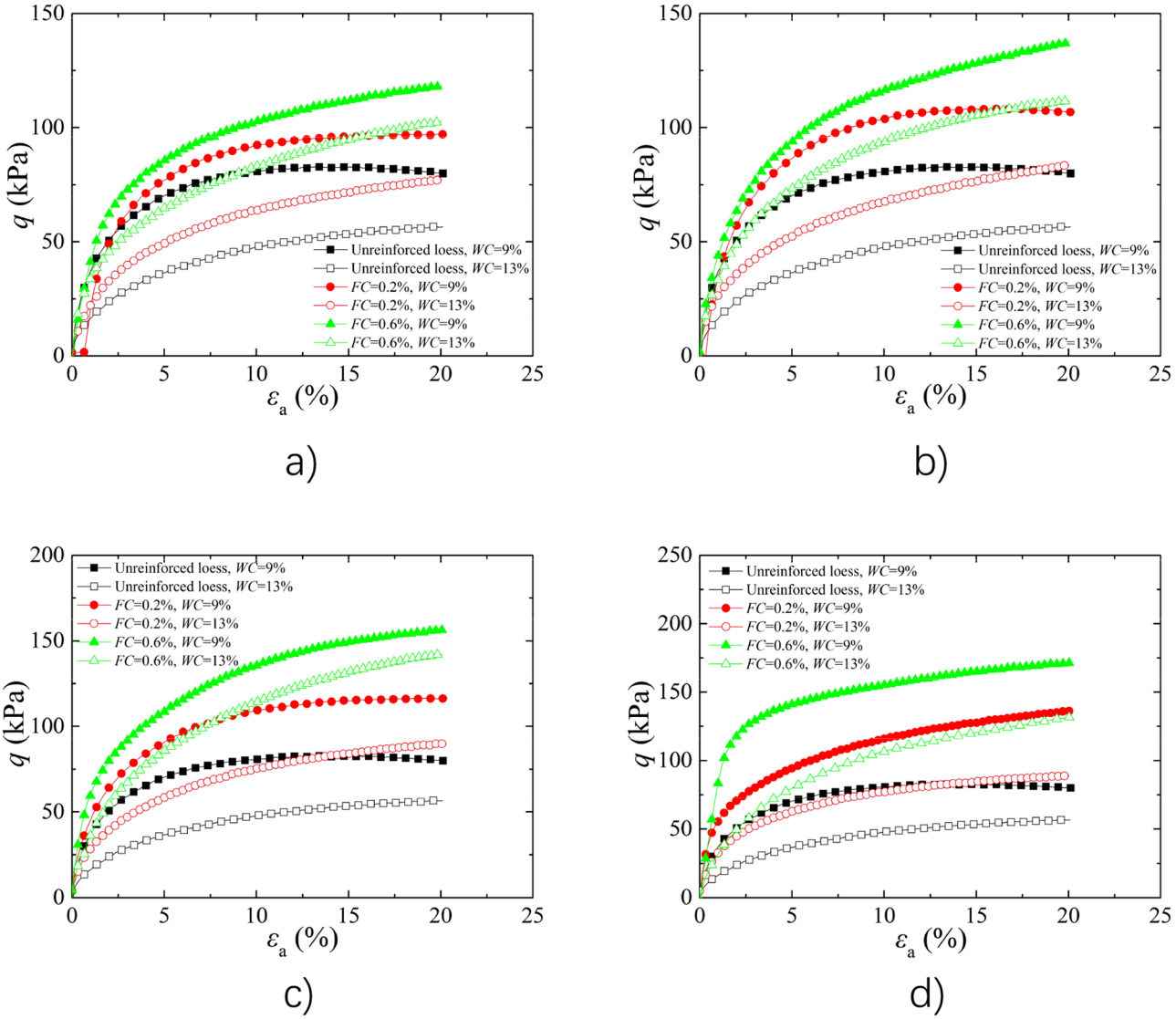

Figure 1. Effect of *w* on stress–strain curves (**a**) *FL* = 4 mm; (**b**) *FL* = 8 mm; (**c**) *FL* = 12 mm; (**d**) *FL* = 16 mm.

Analysis of the Effect of $\boldsymbol{\sigma_3}$

With embed depth increasing, the σ_3 of the soil increased. Figure 4 shows the stress–strain curves of BFR loess with *w* of 9% and *FL* of 4 mm, 8 mm, 12 mm, and 16 mm. The peak strength increased with increasing σ_3, indicating that the strength enhanced with embed depth, which is consistent with the results of the reference[47]. The BFR loess with *FL* and *FC* were 4 mm and 0.2%, the peak strength increased by 61.70% and 173.81% under 50 kPa and 100 kPa σ_3, compared to that under 25 kPa σ_3. Compared with the strength of BFR soil under 25 kPa σ_3, the peak strength increased by 79.94% and 211.01% under 50 kPa and 100 kPa σ_3 when the *FC* of 0.6%, respectively. The main reason is that as σ_3 increased, the constrained of particles increased, and the anchoring effect of fibers by soil particles was enhanced, thereby the sample damage was prevented due to the high tensile strength of fibers, which resulted in the peak deviatoric stress increased and this is in agreement with the experimental results of cement-fiber treated sand[48].

Microstructure characteristics of BFR loess

The microstructure of BFR loess was measured by SEM as listed in Fig. 5. As shown in Fig. 5a, the fiber reinforcement is mainly based on the single tensile effect. The fiber was enveloped by a large number of soil particles. The mutual diastrophism was generated under shear loading result from high tensile strength. Furthermore, interfacial force was produced by the pullout of fibers, and mainly depends on the interfacial friction and adhesion. In the meantime, the restraining effect of fiber on soil particles was produced in the bending part when subject to pullout force, which limited soil deformation and improved shear strength. As shown in Fig. 5b, the fiber reinforcement is mainly based on the spatial mesh structure effect. Many fibers were randomly distributed and interwoven into a mesh structure. When one of the fibers is subject to a tension force, it pulls the other fibers to form a spatial force structure, resulting in the local loading transferred to a broader area, which further

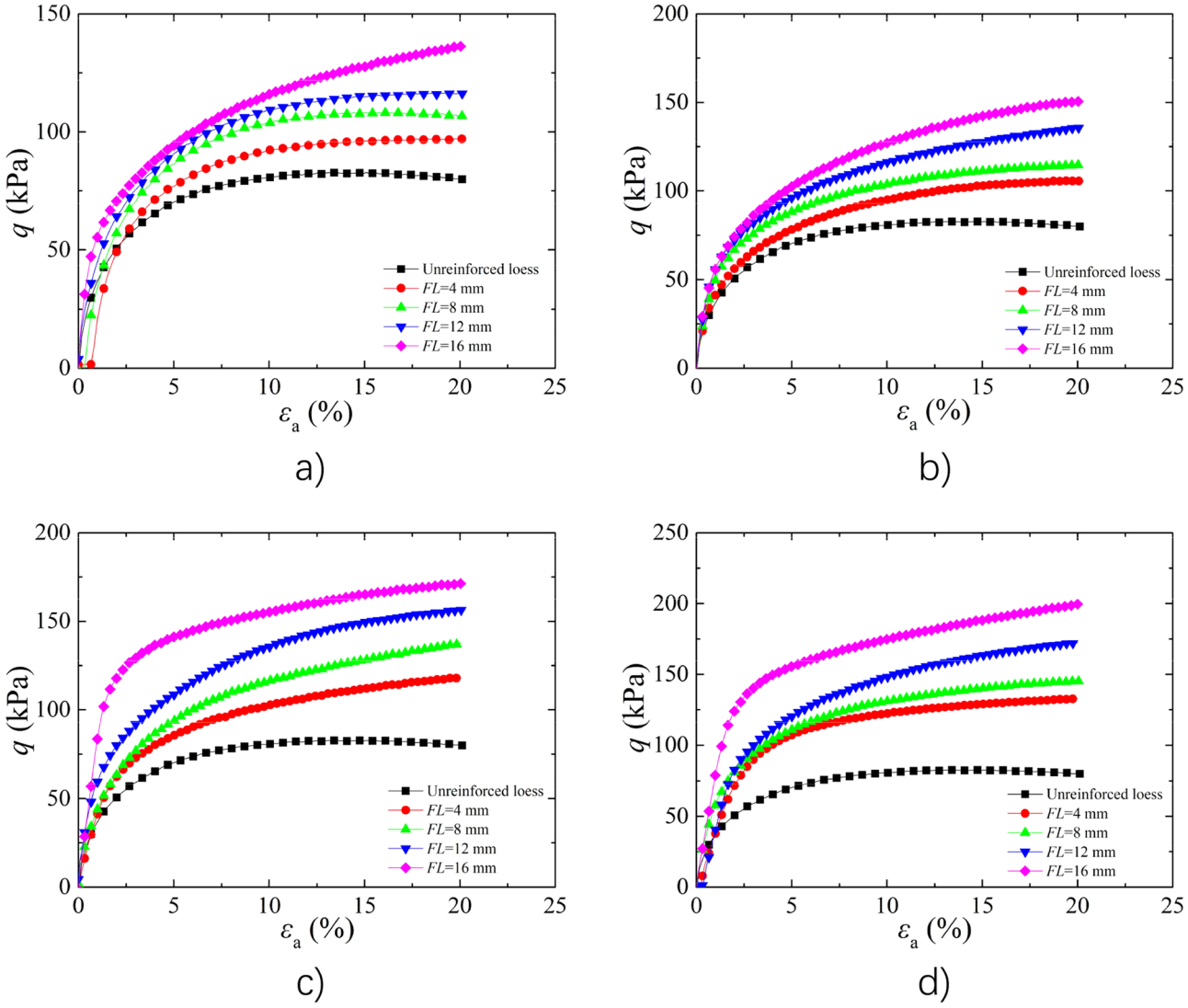

Figure 2. Effect of *FL* on stress–strain curves (**a**) *FC* = 0.2%; (**b**) *FC* = 0.4%; (**c**) *FC* = 0.6%; (**d**) *FC* = 0.8%.

improves the tensile effect of the fibers[49]. In addition, Zhang et al.[50] divided the reinforcement mechanism into bending mechanism and interweaving mechanism. The bending mechanism referred to fibers consisting numerous bends, almost no straight parts. When fiber bearing pullout loading, the friction were generated due to fiber bend. The interweaving mechanism referred to the interweaving points of fibers to form a spatial force structure to limit the displacement, and enhance the overall strength. Liu et al.[51] concluded that the reinforcement mechanism resulted from interface strength, namely friction and cohesion. Furthermore, the interfacial friction primarily depends on the effect of particle shape, particle gradation, interfacial friction coefficient, and effective contact area. The interfacial cohesion mainly depends on the impact of clayey particles, the natural cement, and the interaction friction.

Shear strength model of BFR loess

Model building

The shear strength indices of unreinforced loess and BFR loess are summarized in Table 3. Figure 6a,b shows *FL* affect on the shear strength indices of BFR loess with *w* of 9%. The cohesion of reinforced soil increased as increasing of *FL*, while the internal friction angle changed insignificantly. When *FL* increased from 4 to 8 mm at 0.8% *FC*, the internal friction angle showed decreased trend. The main reason is that when the fiber bend distribution during the soil particles, the tensile strength and friction force cannot fully presented, thereby the internal friction angle may be decreased with increasing *FL*. When the *FC* of 0.8%, the cohesion of the BFR soil increased by 5.3 kPa, 16.1 kPa, 18.7 kPa, and 24.8 kPa with *FL* of 4 mm, 8 mm, 12 mm, and 16 mm, respectively. Figure 6c,d shows *FC* affect on the shear strength indices of BFR loess with *w* of 9%. On the whole, the cohesion of BFR soil increased with increasing *FC*, while internal friction angle varied little. The cohesion changed not significant between 0.2% and 0.4% *FC*, indicating that the reinforcement effect was not evident with low *FC*.

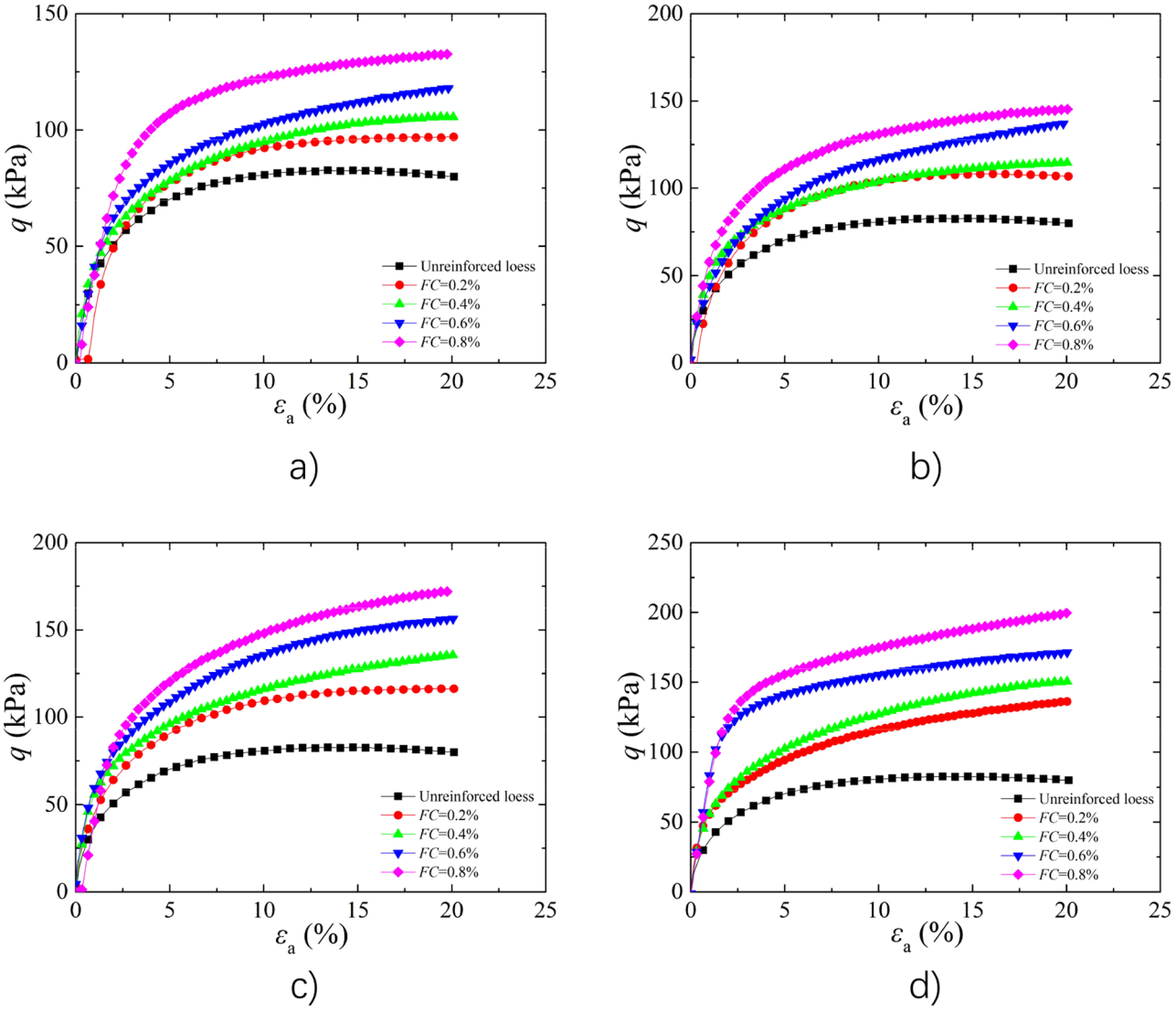

Figure 3. Effect of *FC* on the stress–strain curves (**a**) *FL* = 4 mm; (**b**) *FL* = 8 mm; (**c**) *FL* = 12 mm; (**d**) *FL* = 16 mm.

The reinforcement mechanism of BFR loess is controlled by single tension effect and spatial structure, which formes a force transformation system to bear loading together. According to above research results and taken into account the dimensional effect, it is supposed that the cohesion of reinforced soil c_{FR} is a function of *FL*, and *FC* and *d*.

$$c_{FR} = f\left(\frac{FL \cdot FC}{d}\right) c_0 \tag{1}$$

where c_{FR} and c_0 are cohesive of BFR loess and unreinforced loess, respectively, *FL* is the fiber length, *FC* is the fiber content, and *d* is the fiber diameter.

Equation (1) can be expressed as

$$\frac{c_{FR}}{c_0} = f\left(\frac{FL \cdot FC}{d}\right) \tag{2}$$

By plotting the experimental results as curves of c_{FR}/c_0 versus FL^*FC/d, it was found that c_{FR}/c_0 tends to increase with increasing of FL^*FC/d, and presented a nearly linear relationship, so it is assumed that

$$c_{FR} = \left(a + b \cdot \frac{FL \cdot FC}{d}\right) c_0 \tag{3}$$

where parameters *a* and *b* are the intercept and slope of the fitting curve.

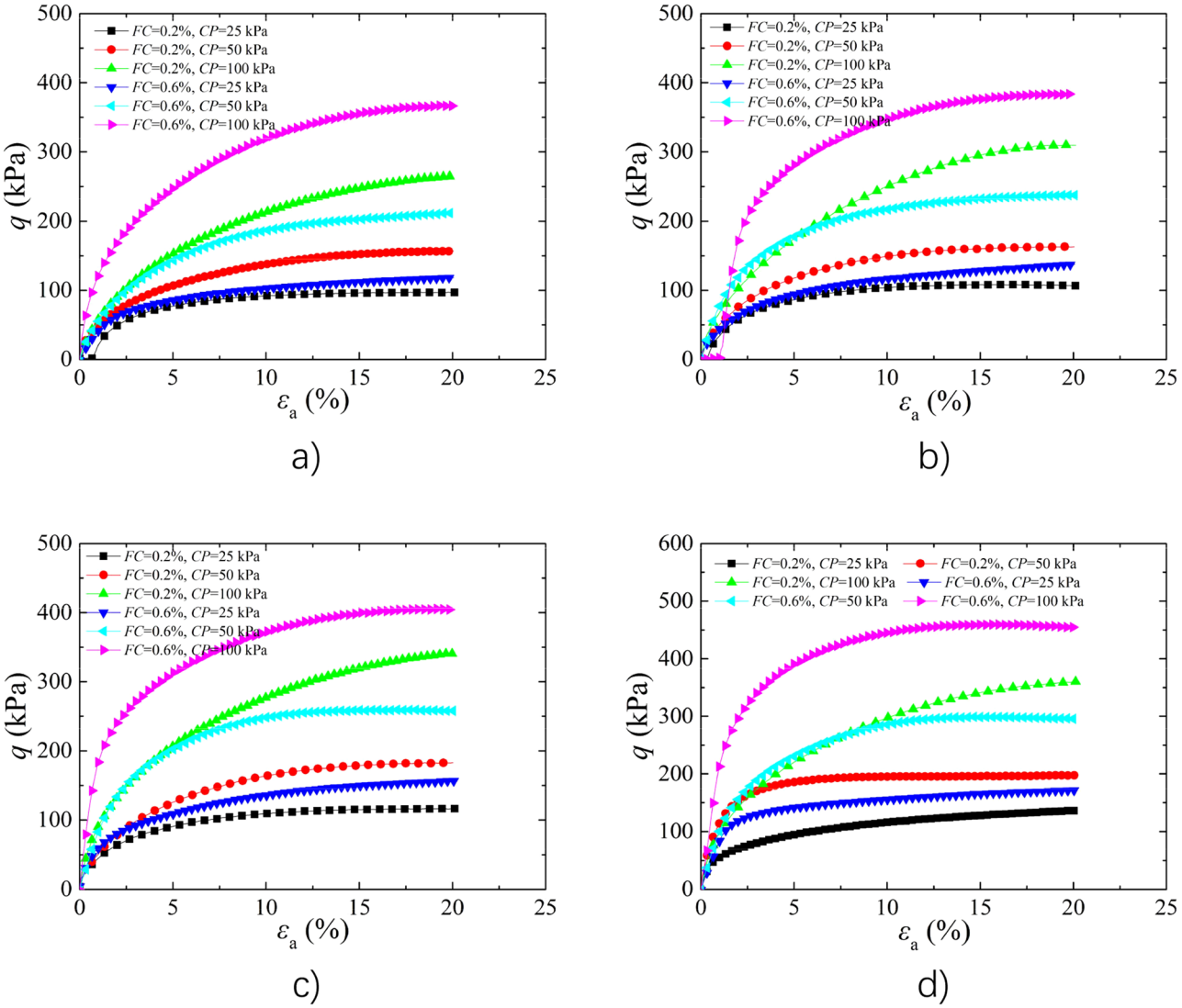

Figure 4. Effect of σ_3 on the stress–strain curves (**a**) $FL = 4$ mm; (**b**) $FL = 8$ mm; (**c**) $FL = 12$ mm; (**d**) $FL = 16$ mm.

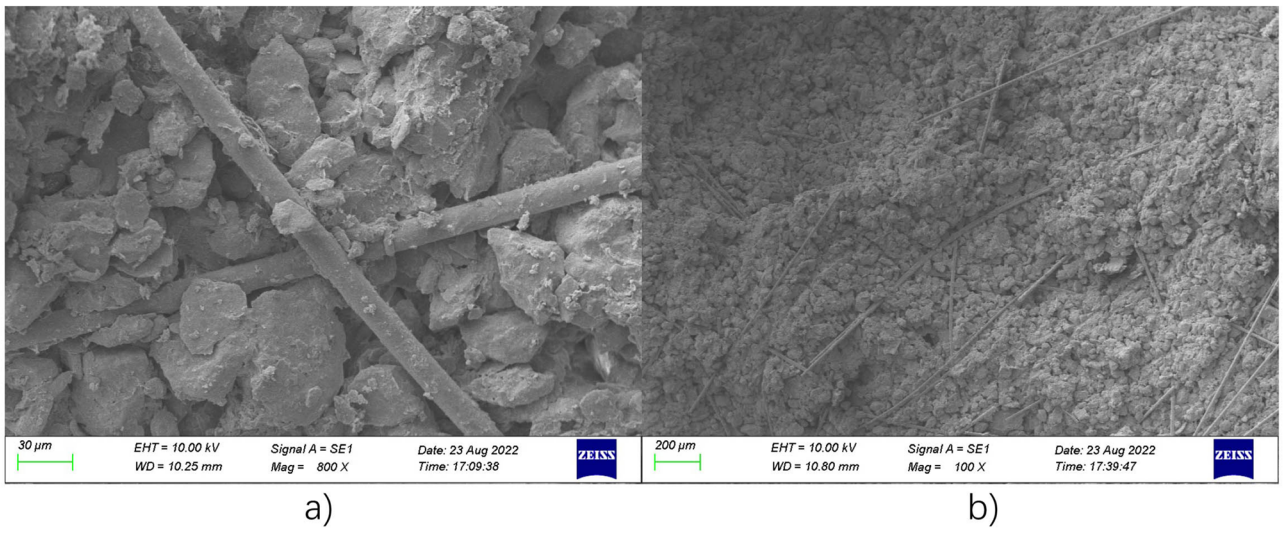

Figure 5. SEM pictures of BFR loess (**a**) Single tensile effect; (**b**) Spatial mesh structure.

w (%)	*FL* (mm)	*FC* (%)	*C* (kPa)	*φ* (°)
9	0	0	8.3	36.5
9	4	0.2	10.9	34.4
9	4	0.4	10.1	37.1
9	4	0.6	13.3	38.4
9	4	0.8	13.6	40.2
9	8	0.2	12.1	35.1
9	8	0.4	12.1	37.2
9	8	0.6	20.2	37.3
9	8	0.8	24.4	37.8
9	12	0.2	13.9	36.1
9	12	0.4	14.2	39.7
9	12	0.6	23.4	38.3
9	12	0.8	27.0	38.8
9	16	0.2	16.9	37.0
9	16	0.4	16.9	39.7
9	16	0.6	24.1	40.7
9	16	0.8	33.1	40.0
13	0	0	6.2	31.8
13	4	0.2	6.7	31.5
13	4	0.4	8.9	31.2
13	4	0.6	10.0	33.4
13	4	0.8	12.6	33.5
13	8	0.2	7.1	31.8
13	8	0.4	10.1	32.6
13	8	0.6	12.6	34.1
13	8	0.8	16.5	33.4
13	12	0.2	8.4	32.0
13	12	0.4	15.2	28.8
13	12	0.6	17.4	33.1
13	12	0.8	19.4	34.2
13	16	0.2	9.3	32.1
13	16	0.4	18.0	30.9
13	16	0.6	18.4	33.8
13	16	0.8	20.8	35.4

Table 3. Shear strength indices of BFR loess.

Compared to unreinforced soil, the internal friction angle varied slightly with increasing *FL* and *FC*, so it is assumed that

$$\tan \varphi_{FR} = \tan \varphi_0 \tag{4}$$

where φ_{FR} and φ_0 are the internal friction angle of BFR and unreinforced soils, respectively.

Based on Mohr–Coulomb theory, combined Eq. (1) with Eq. (4) gained

$$\tau_{FR} = c_{FR} + \tan(\varphi_{FR})\sigma \tag{5}$$

where τ_{FR} is the shear strength of BFR soil, and σ is the stress.

Taking Eq. (3) and Eq. (4) into Eq. (5), we obtained

$$\tau_{FR} = \left(a + b \cdot \frac{FL \cdot FC}{d}\right) c_0 + \tan(\varphi_0)\sigma \tag{6}$$

According to Eq. (6), when the parameters c_0, φ_0, *FL*, *FC*, and *d* are known, the unknown parameters (*a*, *b*) can be obtained using fitting method.

Fitting of model parameters

The Fig. 7 shows the fitting curves of cohesion of BFR loess with 9% and 13% *w*. The value of c_{FR}/c_0 linearly increased as the increasing of *FL***FC*/*d*, and the determined coefficient of the fitting curves reached 0.946 and 0.943 with 9%, 13% *w*, respectively, indicating that the correlation between the horizontal axis and vertical axis

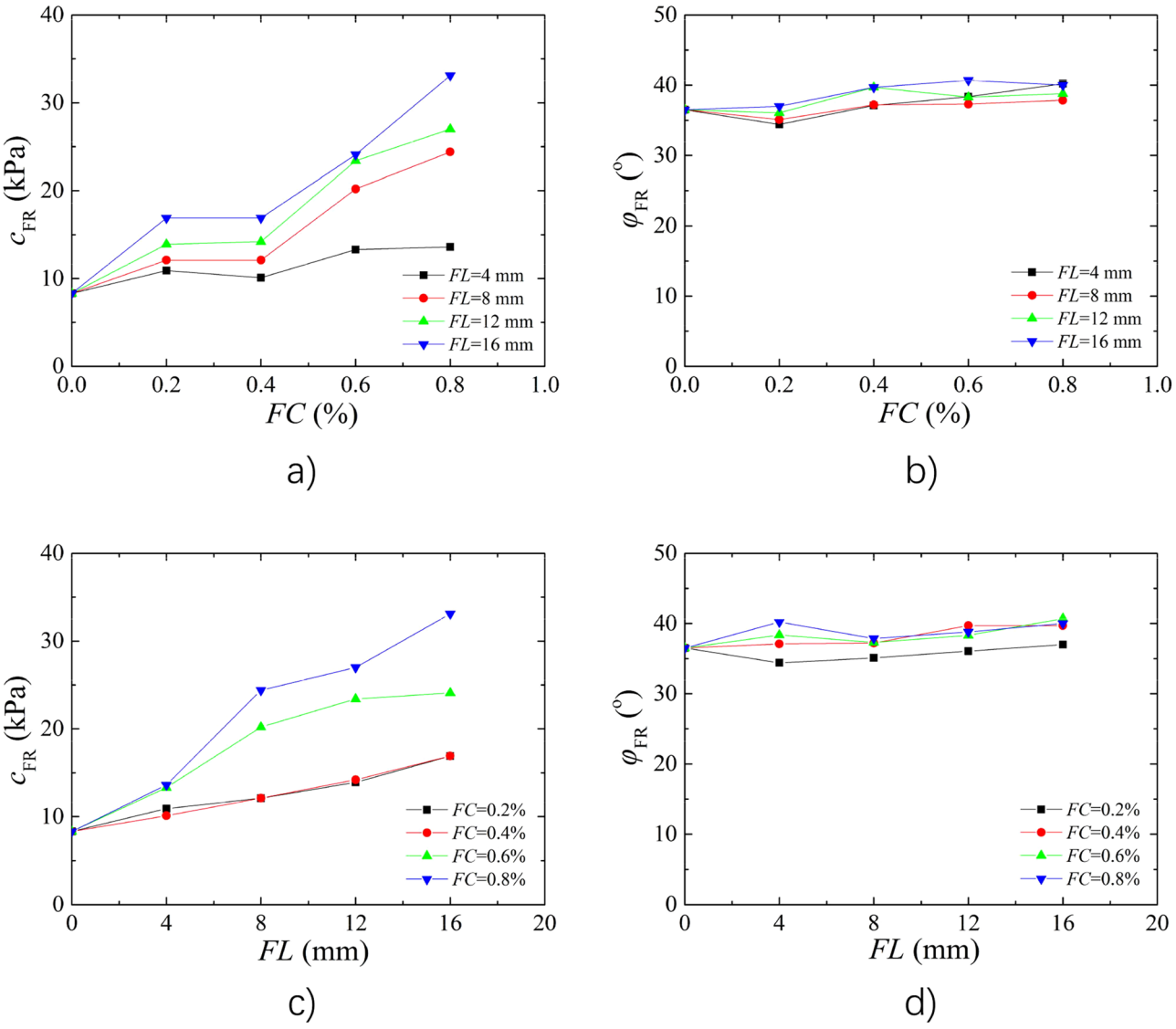

Figure 6. Effect of *FL* and *FC* on shear strength indices (**a**) Effect of *FL* on Cohesion; (**b**) Effect of *FL* on Internal friction angle; (**c**) Effect of *FC* on Cohesion; (**d**) Effect of *FC* on Internal friction angle.

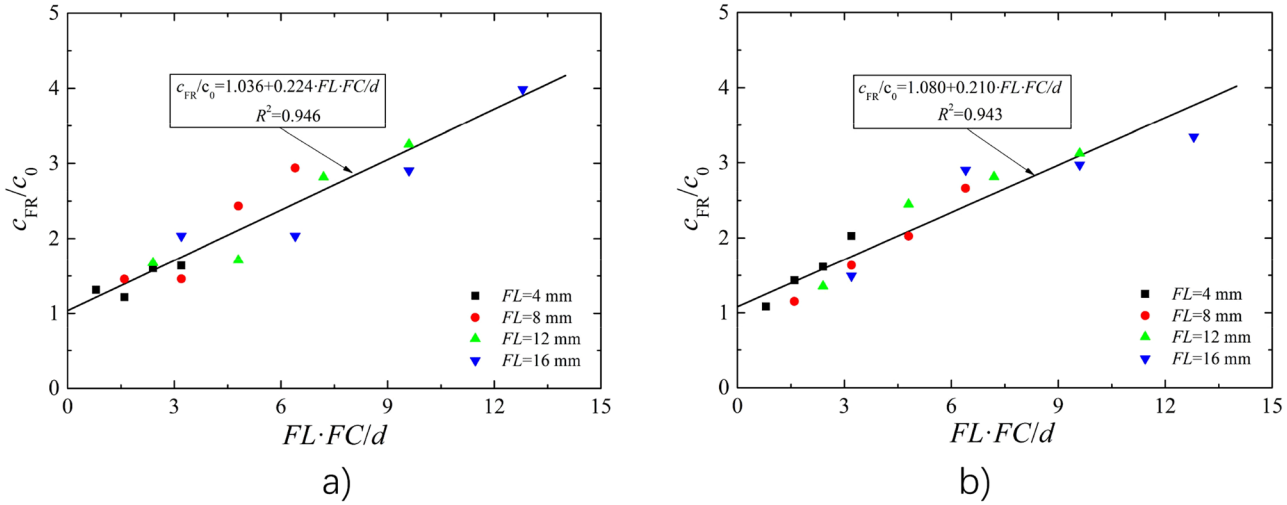

Figure 7. Fitting curves of cohesion (**a**) $w = 9\%$; (**b**) $w = 13\%$.

was good and can be expressed by a linear equation. Overall, considering of intercept a and slope b of the fitting curves with 9% and 13% w, the parameter values were determined as $a = 1.0$ and $b = 0.2$.

Model validation

The parameter values of c_0, FL, FC, and d were known, the cohesive of BFR loess c_{FR} can be obtained by substituting model parameters a and b into Eq. (3), and the τ_{FR} can be obtained by substituting parameters a and b into Eq. (6). Figure 8a,b shows the comparison of cohesion between experimental and predicted. It can be found that the cohesion data were relatively uniformly distributed on two sides of the parallels. Figure 8c,d shows the strength comparison of BFR soil between experimental and predicted. It can be found that the shear strength data were more concentrated and distributed on both sides of the parallels compared to the cohesive data, indicating that the shear strength predicted results agreed better with the experiment results. Based on the comparison of cohesion and shear strength, the predicted values and test values agreed well, which suggested that the model is suitable for predicting the cohesion and shear strength of BFR loess.

Conclusions

According to consolidated undrained tests, the effects of water content (w), fiber length (FL), fiber content (FC), and cell pressure (σ_3) on the shear strength of basalt fiber-reinforced (BFR) loess were investigated. The microstructure characteristics of BFR loess were constructed by SEM test to reveal the reinforcement mechanism of basalt fiber. Furthermore, a shear strength model considering fiber affects was established and verified. The main conclusions were drawn as bellow:

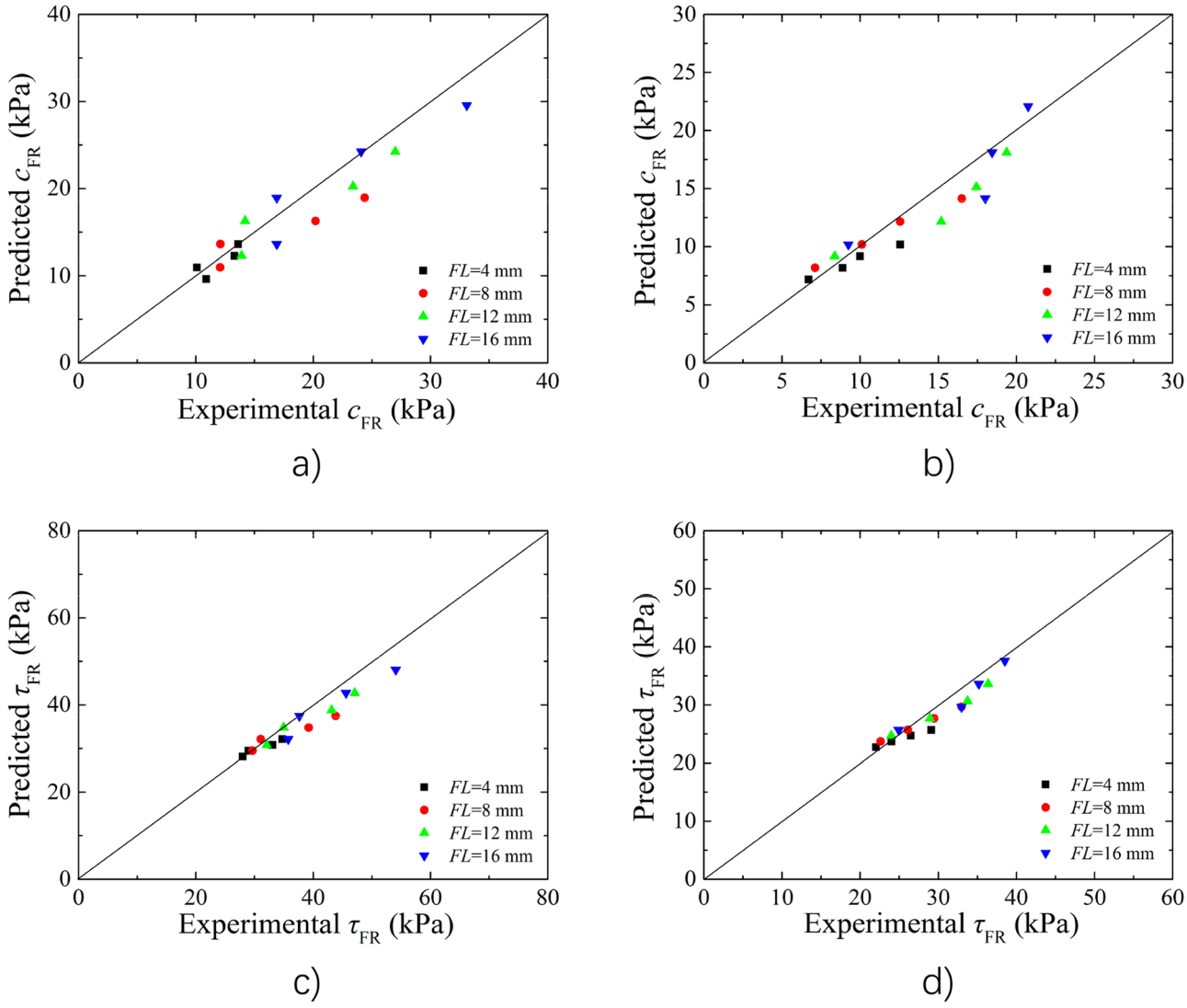

Figure 8. Comparison of the cohesion results and the shear strength results between measured and predicted (**a**) the cohesion results for $w = 9\%$; (**b**) the cohesion results for $w = 13\%$; (**c**) the shear strength results for $w = 9\%$; (**d**) the shear strength results for $w = 13\%$.

(1) The peak strength decreased with increasing *w*, and the BFR loess was remarkably modified compared to unreinforced loess. The peak strength decreased by 20.38% at 13% *w* compared to that at 9% *w* when *FC* was 0.2%.

(2) Loess showed strain-softening, whereas the BFR soils exhibited strain-hardening. With increasing *FL*, the peak strength of BFR soil increased. Compared to unreinforced soil, the peak strength of BFR loess increased by 17.21%, 28.97%, 40.45%, and 64.60% with *FC* was 0.2% and *FL* changed from 4 to 16 mm, respectively.

(3) With increasing *FC*, the peak strength of BFR soils gradually enhanced, and it increased with increasing σ_3. When *FL* was 4 mm and *FC* varied from 0.2% to 0.8%, the peak strength raised by 17.21%, 27.55%, 42.73%, and 60.66%, respectively.

(4) The reinforcement mechanism was controlled by a single tension effect and spatial structure, which combined a force transformation system. When one fiber subject to a tension force, it pulls the other fibers to form a force transformation system, which further improves the overall tensile effect of the fibers.

(5) The optimum reinforcement condition for experimental loess was that of *FL* was 16 mm and *FC* was 0.8%. The predicted results and test results agreed well, which validated the dependability and indicated that the model is suitable to predict the shear strength of BFR loess.

Data availability

All data generated or analysed during this study are included in this published article.

Received: 15 May 2023; Accepted: 21 September 2023
Published online: 23 September 2023

References

1. Zuo, L., Lyu, B., Xu, L. & Li, L. W. The influence of salt contents on the compressibility of remolded loess soils. *Bull. Eng. Geol. Environ.* **81**(5), 185 (2022).
2. Meng, K., Cui, C. Y., Liang, Z. M., Li, H. J. & Pei, H. F. A new approach for longitudinal vibration of a large-diameter floating pipe pile in visco-elastic soil considering the three-dimensional wave effects. *Comput. Geotech.* **128**, 103840 (2020).
3. Cui, C. Y., Zhang, S. P., Chapman, D. & Meng, K. Dynamic impedance of a floating pile embedded in poro-visco-elastic soils subjected to vertical harmonic loads. *Geomech. Eng.* **15**, 793–803 (2018).
4. Cui, C. Y., Meng, K., Wu, Y. J., Chapman, D. & Liang, Z. M. Dynamic response of pipe pile embedded in layered visco-elastic media with radial inhomogeneity under vertical excitation. *Geomech. Eng.* **16**, 609–618 (2018).
5. Hou, Y. F., Li, P. & Wang, J. D. Review of chemical stabilizing agents for improving the physical and mechanical properties of loess. *Bull. Eng. Geol. Environ.* **80**(12), 9201–9215 (2021).
6. Li, G., Zhang, J. L. & Liu, J. Experimental study on the shear behaviors of polypropylene fiber-reinforced sand. *KSCE J. Civ. Eng.* **23**(12), 4992–5001 (2019).
7. Liu, J., Li, X. A., Li, G. & Zhang, J. L. Investigation of the mechanical behavior of polypropylene fiber-reinforced red clay. *Appl. Sci.* **11**(22), 10521 (2021).
8. Ibraim, E. *et al.* Energy efficiency of fibre reinforced soil formation at small element scale: Laboratory and numerical investigation. *Geotext. Geomembr.* **46**, 497–510 (2018).
9. Ibraim, E., Diambra, A., Muir Wood, D. & Russell, A. R. Static liquefaction of fibre reinforced sand under monotonic loading. *Geotext. Geomembr.* **28**, 374–385 (2010).
10. Ibraim, E., Diambra, A., Russell, A. R. & Muir Wood, D. Assessment of laboratory sample preparation for fibre reinforced sands. *Geotext. Geomembr.* **34**, 69–79 (2012).
11. Reza Tabakouei, A., Narani, S. S., Abbaspour, M., Aflaki, E. & Siddiqua, S. Coupled specimen and fiber dimensions influence measurement on the properties of fiber-reinforced soil. *Meas.* **188**, 110556 (2022).
12. Sharma, V. & Kumar, A. Influence of relative density of soil on performance of fiber-reinforced soil foundations. *Geotext. Geomembr.* **45**, 499–507 (2017).
13. Festugato, L., Gálvez, J. H. F., Miguel, G. D. & Consoli, N. C. Cyclic response of fibre reinforced dense sand. *Transp. Geotech.* **37**, 100811 (2022).
14. Choobbasti, A. J., Kutanaei, S. S. & Ghadakpour, M. Shear behavior of fiber-reinforced sand composite. *Arab. J. Geosci.* **12**, 157 (2019).
15. Soriano, I. *et al.* 3D fibre architecture of fibre-reinforced sand. *Granul. Matter.* **19**, 75 (2017).
16. Mandolini, A., Diambra, A. & Ibraim, E. Strength anisotropy of fibre-reinforced sands under multiaxial loading. *Géotechnology* **69**(3), 203–216 (2019).
17. Abdi, M. R., Ghalandarzadeh, A. & Chafi, L. S. An investigation into the effects of lime on compressive and shear strength characteristics of fiber-reinforced clays. *J. Rock Mech. Geotech. Eng.* **13**, 885–898 (2021).
18. Hejazi, S. M., Sheikhzadeh, M., Abtahi, S. M. & Zadhoush, A. Shear modeling of fiber reinforced soil composite on the base of fiber pull-out test. *Fib. Polym.* **14**(2), 277–284 (2013).
19. Abbaspour, M., Narani, S. S., Aflaki, E., Moghadas Nejad, F. & Mir Mohammad Hosseini, S. M. Strength and swelling properties of a waste tire textile fiber-reinforced expansive soil. *Geosynth. Int.* **27**(5), 476–489 (2020).
20. Consoli, N. C., Bellaver Corte, M. & Festugato, L. Key parameter for tensile and compressive strength of fibre-reinforced soil-lime mixtures. *Geosynth. Int.* **19**(5), 409–414 (2012).
21. Consoli, N. C., Festugato, L., Miguel, G. D. & Scheuermann Filho, H. C. Swelling prediction for green stabilized fiber-reinforced sulfate-rich dispersive soils. *Geosynth. Int.* **28**(4), 391–401 (2021).
22. Tamassoki, S. *et al.* Compressive and shear strengths of coir fibre reinforced activated carbon stabilised lateritic soil. *Sustainability* **14**, 9100 (2022).
23. Soleimani-Fard, H., Konig, D. & Goudarzy, M. Plane strain shear strength of unsaturated fiber-reinforced fine-grained soils. *Acta Geotech.* **17**, 105–118 (2022).
24. Malekzadeh, M. & Bilsel, H. Hydro-mechanical behavior of polypropylene fiber reinforced expansive soils. *KSCE J. Civ. Eng.* **18**(7), 2028–2033 (2014).
25. Phanikumar, B. R. & Singla, R. Swell-consolidation characteristics of fibre-reinforced expansive soils. *Soils Found.* **56**(1), 138–143 (2016).
26. Wang, K. T., Zhang, L. X., Wang, Y. T. & Chang, Z. M. Study on the influence of glass fibre on the mechanical properties of collapsible loess. *Water Power.* **46**(10), 117–121 (2020).
27. Huang, J. H., Bao, F., Li, H. & Yang, J. Experimental study on mechanical properties of glass fiber-reinforced loess. *Yangtze River* **51**(S2), 260–264 (2020).

28. Xu, J., Wu, Z. P. & Chen, H. Triaxial shear behavior of basalt fiber reinforced loess under drying-wetting cycles. *Rock Soil Mech.* **43**(1), 28–36 (2022).
29. Zhu, M., Ni, W. K., Li, X. N., Wang, H. M. & Zhao, L. Study on unconfined compressive strength and deformation after incorporating polypropylene fiber into loess. *Sci. Technol. Eng.* **20**(20), 8337–8343 (2020).
30. Zuo, C. X., Sun, S. L., Huang, M. J., Gao, S. Q. & Zhang, Y. Experimental study on loess compressive strength improvement through xanthan gum and basalt fiber. *Coal Geol. China* **34**(1), 57–61 (2022).
31. Lu, H. *et al.* Shear strength and disintegration properties of polypropylene fiber-reinforced loess. *J. Traffic Transp. Eng.* **21**(2), 82–92 (2021).
32. An, N. *et al.* Experimental study on anti-erosion performance of polypropylene fiber-reinforced loess. *Rock Soil Mech.* **42**(2), 501–510 (2021).
33. Dong, C. F., Zhang, W. Y., Sun, X. L. & Xie, B. L. Experimental study on the shear strength of lignin fiber-improved loess. *Saf. Environ. Eng.* **29**(2), 102–110 (2022).
34. Chu, F., Zhang, H. G., Shao, S. J. & Deng, G. H. Experimental study on mechanical deformation and corrosion resistance characteristics of loess reinforced with synthetic waste cloth fiber yarn. *Rock Soil Mech.* **41**(S1), 394–403 (2020).
35. Xiong, Y., Deng, H. F., Peng, M., Qi, Y. & Li, T. Shear properties of loess reinforced with four synthetic fibers. *J. Yangtze River Sci. Res. Inst.* **39**(1), 122–133 (2022).
36. Wang, G. G., Luo, Y. S., Li, P. D. & Zhao, Y. B. Experimental study on three axis creep of fiber reinforced loess. *Sci. Technol. Eng.* **20**(19), 7602–7608 (2020).
37. Hu, W. L., He, P. L. & Liu, H. Experimental study on optimization of shear strength parameters of basalt fiber loess. *The Chin. J. Geol. Hazard Control* **30**(4), 92–97 (2019).
38. Gao, Z. N. *et al.* Effect of mixing method of sample preparation on the strength of loess improved by lignin fiber. *China Earthq. Eng. J.* **43**(4), 930–934 (2021).
39. Su, S. & Lei, S. Y. Experimental study on tensile and compressive properties of palm fiber loess. *China Sci. Pap.* **15**(12), 1391–1394 (2020).
40. Chen, S. F., Luo, T., Li, G. & Zhang, Y. Effects of cyclic freezing-thawing on dynamic properties of loess reinforced with polypropylene fiber and fly ash. *Water* **14**(3), 317 (2022).
41. Yang, B. H. *et al.* Strength characteristics of modified polypropylene fiber and cement-reinforced loess. *J. Cent. South Univ.* **24**(3), 560–568 (2017).
42. GB/T 50123–2019; Standard for soil test method. (Construction Ministry of PRC, 2019).
43. Arabani, M. & Haghsheno, H. The effect of water content on shear and compressive behavior of polymeric fiber-reinforced clay. *SN Appl. Sci.* **2**, 1759 (2020).
44. Zhao, F. T. & Zheng, Y. W. Shear strength behavior of fiber-reinforced soil: experimental investigation and prediction model. *Int. J. Geomech.* **22**(9), 04022146 (2022).
45. Dehghan, A. & Hamidi, A. Triaxial shear behaviour of sand-gravel mixtures reinforced with cement and fibre. *Int. J. Geotech. Eng.* **10**(5), 510–520 (2016).
46. Shen, Y. S., Tang, Y., Yin, J., Li, M. P. & Wen, T. An experimental investigation on strength characteristics of fiber-reinforced clayey soil treated with lime or cement. *Constr. Build. Mater.* **294**, 123537 (2021).
47. Hou, T. S., Liu, J. L., Luo, Y. S. & Cui, Y. X. Triaxial compression test on consolidated undrained shear strength characteristics of fiber reinforced soil. *Soils Rocks* **43**(1), 43–55 (2020).
48. Hamidi, A. & Hooresfand, M. Effect of fiber reinforcement on triaxial shear behavior of cement treated sand. *Geotext. Geomembr.* **36**, 1–9 (2013).
49. Wang, D. Y. *et al.* Shear strength characteristics of fiber-reinforced unsaturated cohesive soils. *Chin. J. Geotech. Eng.* **35**(10), 1933–1940 (2013).
50. Zhang, Y. M., Zhang, X. D. & Zhang, H. R. Test research of geotechnique textile soil reinforcement mechanism and engineering application. *Rock Soil Mech.* **26**(8), 1323–1326 (2005).
51. Liu, B. S. *et al.* Advances in engineering properties of fiber reinforced soil. *J. Eng. Geol.* **21**(4), 540–547 (2013).

Acknowledgements

This study was supported by the Natural Science Basic Research Program of Shaanxi Province (2021JM-535, 2023-JC-QN-0277 and 2023-JC-QN-0322), Young Talent Fund of Association for Science and Technology in Shaanxi, China (20220719), and Special Fund for Scientific Research by Xijing University (XJ18T01 and XJ22B05).

Author contributions

C-K.C. and G.L. initiated the study. J.L. designed the scope of study. Y.X. and J.-J.N. reviewed and edited the manuscript.

Competing interests

The authors declare no competing interests.

Additional information

Correspondence and requests for materials should be addressed to G.L.

Reprints and permissions information is available at www.nature.com/reprints.

Publisher's note Springer Nature remains neutral with regard to jurisdictional claims in published maps and institutional affiliations.